

LONG-TERM X-RAY SPECTRAL VARIABILITY OF THE RADIO-LOUD NLS1 GALAXY PKS 0558–504

M. GLIOZZI

George Mason University, 4400 University Drive, Fairfax, VA 22030

I.E. PAPADAKIS

Physics Department, University of Crete, 710 03 Heraklion, Crete, Greece

W.P. BRINKMANN

Max-Planck-Institut für extraterrestrische Physik, Postfach 1312, D-85741 Garching, Germany

Draft version October 30, 2018

ABSTRACT

We present X-ray observations of the Narrow-Line Seyfert 1 galaxy PKS 0558–504 obtained with *RXTE* during a 1-year monitoring campaign. This source, which is one of the very few radio-loud NLS1 galaxies, shows strong X-ray flux variability on time scales of weeks-months accompanied by spectral variability. The main goal of this study is to investigate the spectral variability with model-independent methods and time-resolved spectroscopy in order to shed light on the origin of the X-rays. The main results can be summarized as follows: 1) The flux typically changes by a factor of 1.5–2 on time scales of 10–30 days, with few extreme events where the flux increases by a factor of ~ 4 in 3 days. 2) We do not observe any large amplitude, flux related spectral variations. During the flux variations, the spectrum varies mainly in normalization and not in shape. We do observe some small amplitude spectral variations, which do not correlate with flux, although there is a hint of spectral hardening as the source brightens. 3) There is no evidence for reprocessing features such as the Fe $K\alpha$ line or a Compton hump. We argue that PKS 0558–504 is a peculiar object that appears to be different from most of the radio-quiet and radio-loud AGN. If a jet is responsible for the bulk of the X-rays, it must operate in an unusual way. If instead a corona is responsible for the X-rays, the system might be a large-scale analog of the Galactic black holes in the transient intermediate state.

Subject headings: Galaxies: active – Galaxies: jets – Galaxies: nuclei – X-rays: galaxies

1. INTRODUCTION

Narrow-Line Seyfert 1 galaxies (NLS1) are identified by their optical emission line properties: the ratio $[O\ III]/H\beta$ is less than 3 and FWHM $H\beta$ is less than 2000 km s^{-1} (Osterbrock & Pogge 1985, Goodrich 1989). NLS1 exhibit characteristic features at other wavelengths as well: they are usually strong infrared emitters (Moran et al. 1996) and they are seldom radio loud (Ulvestad et al. 1995, Siebert et al. 1999, Grupe et al. 1999, 2000). The latter result has been recently confirmed by Komossa et al. (2006) who performed a systematic search of radio-loud NLS1s, finding that less than 7% have radio-loudness factors $R > 10$ and only 2.5% have $R > 100$. In the X-rays NLS1 have been generally found to have extreme spectral and variability properties (e.g., Puchnarewicz et al. 1992; Forster & Halpern 1996; Boller et al. 1997; Brandt et al. 1999; Leighly 1999a,b; Grupe et al. 2001). It is now generally accepted that NLS1 are AGN in their early phase (Grupe et al. 1999; Mathur 2000), characterized by relatively small black hole masses (e.g., Grupe & Mathur 2004), and very high accretion rates in terms of Eddington units (e.g., Boroson & Green 1992; Sulentic et al. 2000; Grupe 2004).

PKS 0558–504 ($z = 0.137$, $m_B = 14.97$) is one of the few radio-loud NLS1 galaxies ($R_L = f_{5\text{GHz}}/f_B \simeq 27$, Siebert et al. 1999). It was optically identified on the basis of X-ray positions from the High Energy Astronomy Observatory (HEAO-1, Remillard et al. 1986). Based on the empirical correlation between the broad line region (BLR) and the

optical luminosity (Kaspi et al. 2000), and assuming that the BLR is virialized, Wang et al. (2001) derived a black hole mass of $4.5 \times 10^7 M_\odot$ for PKS 0558–504.

Previous X-ray observations with different satellites have confirmed that PKS 0558–504 shows the characteristic NLS1 properties: strong variability, steep X-ray spectrum, substantial soft excess, and relatively high luminosity. By comparing the X-ray observations throughout the last decade, it is evident that the strong X-ray variability of PKS 0558–504 occurs persistently but without being accompanied by significant spectral variability: the spectrum above 2 keV is consistently described by a power-law model with photon index $\Gamma \sim 2.2$ (Gliozzi et al. 2000).

PKS 0558–504 has been observed repeatedly by *XMM-Newton* as a calibration and performance verification target. A spectral analysis of the first *XMM-Newton* observations (O’Brien et al. 2001) indicates that the broad-band spectrum is well fitted by a Comptonization model. This is in substantial agreement with the findings of Brinkmann et al. (2004), who, analyzing several *XMM-Newton* observations of PKS 0558–504, proposed a scenario with two Comptonization components: one with high temperature and low optical depth ($kT \gtrsim 50\text{ keV}$, $\tau \sim 0.7$), typical of “normal” broad-line Seyfert galaxies, and an additional cooler component with larger optical depth ($kT \sim 4.5\text{ keV}$, $\tau \gtrsim 2$). On the other hand, this interpretation is in sharp contrast with the scenario proposed by Ballantyne et al. (2001) and Crummy et al. (2006) who hypothesize the dominant role played by a highly ionized reflector, based

on ASCA and *XMM-Newton* spectral data, respectively. In any case, since the two competing models have spectral parameters poorly constrained, neither of them can be firmly ruled out.

A temporal analysis of the first *XMM-Newton* observations of PKS 0558–504 (Gliozzi et al. 2001) showed persistent X-ray variability with a tendency of the X-ray spectrum to harden when the count rate increases. A similar spectral variability has been observed in another radio-loud NLS1, RX J0134-4258 (Grube et al. 2000) and in the NLS1 1H 0707-495 (Gallo et al. 2004). This trend is rather unusual for Seyfert galaxies, which generally show an opposite behavior (e.g., Papadakis et al. 2002), instead, it is more typical for jet-dominated sources (e.g., Fossati et al. 2000; Gliozzi et al. 2006a). Indeed, the contribution of the beamed emission from a putative jet has been proposed in the past (Remillard et al. 1991) as possible cause for the brightness and extreme short-term variability of PKS 0558–504 in the X-rays. However, Brinkmann et al. (2004) have shown that this unusual spectral trend seem to be present only sporadically and preferentially at relatively high count rates. This suggests that the X-ray emission from PKS 0558–504 can be the results of a “normal” Seyfert-like and a jet component emerging only during the high state.

In this paper, we start a systematic study of the long-term X-ray flux and spectral variability of PKS 0558–504 using proprietary Rossi X-ray Timing Explorer (*RXTE*) observations in the 2–15 keV range (i.e., in an energy band beyond the X-ray soft excess). We use several model-independent methods to study the X-ray temporal and spectral properties of this source. One of the main purposes of this analysis is to shed light on the origin of the X-rays and in particular on the role played by a jet in the X-rays. Once the jet contribution is properly assessed, the physical parameters characterizing the accretion process onto the supermassive black hole can be better constrained, and hence it is possible to discriminate between competing theoretical models.

This model-independent characterization of a possible jet contribution at X-rays is important not only for radio-loud AGN, but also for their scaled-down counterparts, the Galactic black holes (GBHs), which are known to have compact radio jets during their “low-hard” spectral state. Also in the “very-high” state, radio emission is observed but in the form of optically thin radio flares which are thought to be signatures of powerful ejection events often resolved as extended jets (e.g., Mirabel & Rodriguez 1994). Despite the much higher signal-to-noise of their spectra and light curves, the jet contribution to the total X-ray emission in GBHs is still matter of strong debate (see, e.g., Markoff et al. 2003; Zdziarski et al. 2004).

The outline of the paper is as follows. In § 2 we describe the observations and data reduction. The main characteristics of the X-ray light curve are described in § 3. In § 4 we study the X-ray spectral variability of PKS 0558–504 with several model-independent methods. In § 5 we describe the results of a time-resolved spectral analysis. In § 6 we summarize the main results and discuss their implications.

2. OBSERVATIONS AND DATA REDUCTION

We use proprietary *RXTE* data of PKS 0558–504 that was observed between 2005 March 4 and 2006 March 2. A second monitoring campaign is currently underway. Both campaigns are performed with similar sampling: for 11 months PKS 0558–504 is regularly observed for ~ 1000 – 2000 s once every 2 days, while for one month 2 pointings per day are performed. The observations were carried out with the Proportional Counter Array (PCA; Jahoda et al. 1996), and the High-Energy X-Ray Timing Experiment (HEXTE; Rothschild et al. 1998) on *RXTE*. Here we will consider only PCA data, because the signal-to-noise of the HEXTE data is too low for a meaningful analysis.

The PCA data were screened according to the following acceptance criteria: the satellite was out of the South Atlantic Anomaly (SAA) for at least 30 minutes, the Earth elevation angle was $\geq 10^\circ$, the offset from the nominal optical position was $\leq 0^\circ 02$, and the parameter ELECTRON-2 was ≤ 0.1 . The last criterion removes data with high particle background rates in the Proportional Counter Units (PCUs). The PCA background spectra and light curves were determined using the L7–240 model developed at the *RXTE* Guest Observer Facility (GOF) and implemented by the program `pcabackest v.2.1b`. This model is appropriate for “faint” sources, i.e., those producing count rates less than $40 \text{ s}^{-1} \text{ PCU}^{-1}$.

All the above tasks were carried out using the FTTOOLS v.5.3.1 software package and with the help of the REX script provided by the *RXTE* GOF. Data were initially extracted with 16 s time resolution and subsequently re-binned at different bin widths depending on the application. The current temporal analysis is restricted to PCA, STANDARD-2 mode, 2–15 keV, Layer 1 data, because that is where the PCA is best calibrated and most sensitive. PCUs 0 and 2 were turned on throughout the monitoring campaign. However, since the propane layer on PCU0 was damaged in May 2000, causing a systematic increase of the background, we conservatively use only PCU2 for our analysis (see below). All quoted count rates are therefore for one PCU.

The spectral analysis of PCA data was performed using the XSPEC v.11.3.1 software package (Arnaud 1996). We used PCA response matrices and effective area curves created specifically for the individual observations by the program `pcarsp`, taking into account the evolution of the detector properties. All the spectra were re-binned so that each bin contained at least 20 counts for the χ^2 statistic to be valid. Fits were performed in the energy range 3–15 keV, where the signal-to-noise ratio is the highest.

3. THE X-RAY LIGHT CURVES

Figure 1 shows the background-subtracted, 2–15 keV light curves of PCU0 (top panel), PCU2 (middle panel), and their ratio (bottom panel) with a time bin of 2 days. A visual inspection of the bottom panel in this Figure suggests that the PCU0 and PCU2 light curves are broadly consistent with each other, with the former being characterized by a higher count rate. However, a formal check based on a χ^2 test indicates that the ratio PCU0/PCU2 is not consistent with the hypothesis of constancy ($\chi^2 = 222.7$ for 143 degrees of freedom, hereafter dof). Since the propane layer on PCU0 was damaged a few years ago, we decided to work with the PCU2 data

only. We note though that we also performed the same data analysis on the PCU0 data, and the results are in broad agreement with those from the PCU2.

Both the PCU0 and PCU2 light curves look similar to other long-term, RXTE monitoring light curves of Seyfert galaxies (see Markowitz & Edelson 2001 for a review). There are variations on all sampled time scales, with typical amplitude (max-min)/min of the order of ~ 1.5 –2 over 1 week – 10 days, and several peaks with the most prominent occurring ~ 100 days after the start of the monitoring campaign. These variations appear to be erratic, and we cannot easily identify any well defined, long-term trend, like “flare-like” events, or long-term flux decay/rise trends. The analysis of the flux variations using “traditional” (i.e. power spectrum analysis) and “non-traditional” techniques (e.g., Gliozzi et al. 2006b) will be presented in the future after completion of the second monitoring campaign. Here we limit ourselves to the analysis of the spectral variability of the first year of *RXTE* observations of PKS 0558–504.

To this end, we constructed background subtracted light curves in two energy bands, namely the “soft” (2.5–5 keV) and the “hard” (5–15 keV) band. We show them in Figure 2, together with the hardness ratio (hard/soft). Time bins are two days. As mentioned in the previous section, the PKS 0558–504 *RXTE* observations were carried out following two different sampling patterns, in order to probe as many time scales as possible and hence estimate the power spectral density as accurately as possible. It is likely that in disk and/or jet systems, different physical processes may be at work on different time scales. For example, one may expect that the quite different (in magnitude) viscous, thermal, and dynamical time scales (associated with the accretion process), heating and reprocessing time scales (associated with the disk-corona interactions), or, in the case of jet-dominated objects, the cooling and acceleration time scales of relativistic electrons, may play a role. For this reason, we first treat separately the data from “sampling period 1” (hereafter S1: eleven months with one observation every 2 days) and “sampling period 2” (S2: one month with two observations per day), using time bins of 5760 s (~ 1 *RXTE* orbit). If the results are consistent (as it is the case for PKS 0558–504; see below), we combine the two data sets and repeat the analysis using time bins of two days to increase the significance of the results.

The soft and hard band light curves appear to be quite similar, with the same variations appearing in them. This is also implied by the hardness ratio light curve, which appears to be roughly constant. However, a χ^2 test against the hypothesis of constant hardness ratio implies significant spectral variations. We find that $\chi^2 = 224.4/140$ dof (using separate samplings: $\chi^2 = 247.3/166$ dof and $\chi^2 = 116/53$ dof for the S1 and S2 data, respectively). We have computed the fractional variability (see §4.3 for more details) for the soft, hard, and *HR* light curves: $F_{\text{var,soft}} = 0.31 \pm 0.01$, $F_{\text{var,hard}} = 0.29 \pm 0.01$, $F_{\text{var,HR}} = 0.08 \pm 0.02$. The variability amplitude is roughly similar in both bands, whereas the amplitude of the spectral variations is much smaller. We conclude that the flux variations in PKS 0558–504 are associated with spectral variations which are significant, although of smaller amplitude.

4. SPECTRAL VARIABILITY: MODEL-INDEPENDENT ANALYSIS

Previous X-ray studies, based mainly on time-averaged spectral studies, have offered different interpretations of the physical origin of the X-rays in PKS 0558–504. Our main aim in this work is to investigate whether the study of the source’s X-ray spectral variability can help us clarify the situation.

We begin our study with the use of simple methods and tools like flux-flux plots, hardness ratio versus count rate plots, and the fractional variability versus energy plots. These can provide useful information without any a priori assumption regarding the shape of the X-ray continuum spectrum. Thus, the results from the study of these plots can be considered as “model-independent”.

In the following analyses we fit various data sets with linear functions, using the the routine `fitexy` (Press et al. 1997) that accounts for the errors not only on the y-axis but along the x-axis as well. In many plots, we observe that the data follow a linear trend, but with substantial scatter around it. In this case, in order to reveal clearly the underlying trend, we bin the data using count rate bins of fixed size (0.1 counts/s), and compute the weighted mean (along both the y and x-axis) of all the points which fall into a bin. The error on the weighted mean is computed following Bevington’s prescriptions (Bevington 1969).

4.1. The Flux-Flux Plot

This simple method of plotting the hard versus the soft X-ray count rate can be used to investigate the presence of spectral variations (Churazov et al. 2001; Taylor et al. 2003). For example, if the flux-flux plot of an object is well described by a simple linear model (i.e. a straight line) then the continuum varies only in normalization and not in shape. Furthermore, if the intercept of the y-axis is non-zero, then there also exists a second spectral component, which is non variable, neither in shape nor in normalization. On the other hand, if the flux-flux plot is best described by a non-linear function (a power law for example), then the observed flux variations should be associated with spectral variations as well, i.e. we may be dealing with a power-law like continuum with variable normalization and photon index as well.

We made a flux-flux plot for PKS 0558–504 (see Fig. 3) using the 2.5–5 keV and 5–15 keV light curves as representative of the “soft” and “hard” energy band flux, respectively. The gray (light blue in color) symbols represent the original data with time bins of two days.

A visual inspection of Fig. 3 clearly shows that there exists a linear relationship between the soft and hard flux (this is true also for the separate S1 and S2 data sets). However, the fit of the simple linear model is poor, due to the scatter in the hard flux values for a given soft flux count rate. Nevertheless, the scatter is small and contains no systematic deviations from a linear model. To verify this, we have also plotted the binned data (black filled circles in Fig. 3) together with the best-fit linear models. The linear model fits the binned data very well, and the best fitting results for binned data sets are consistent with each other. In all cases (S1, S2, and combined data sets) the y-axis intercept is consistent with zero. Similar results are obtained when we use other bands (either than 5–15 keV)

as representative of the high energy band. In all cases, the soft vs. hard band plots are well fitted, on average, by straight lines with almost zero y -axis intercepts. The best fitting results are listed in Table 1.

In conclusion, we find that the hard and soft band light curves are very well correlated. On average, this correlation is well described by a simple linear relation with intercept around zero. This relation is the same for both the S1 and S2 data sets, which implies that the source behaves in the same way during the long (weeks, years) and shorter (days) time scales. The linear hard vs soft relation is consistent with a power-law like X-ray continuum which is variable only in normalization and not in shape. The zero y -axis intercept also suggests that there is no indication of an extra, constant component (like e.g. the constant disk-reflection component that has been detected in the X-ray spectra of a few nearby AGN). When we examine the full data sets, we find moderate scatter of the points around the underlying, linear, hard vs soft relation. This result implies some weak spectral variability which is uncorrelated with flux.

4.2. Hardness Ratio vs. Count Rate

Figure 4 shows the Hard/Soft X-ray color plotted versus the count rate for unbinned (gray/blue crosses) and binned data (black symbols), respectively. A visual inspection of Figure 4 clearly shows that the hardness ratio does not appear to correlate with the count rate (S2 and S1 data sets are virtually indistinguishable in this analysis). However, when we fit a simple linear model to the data, we do observe a weak positive correlation (see Table 1). The best fitting slope is 0.05 ± 0.02 , which is a 2.5σ effect.

Better insight in the presence of correlations between HR and total count rate can be obtained by investigating the binned data (black circles in Fig. 4). In this case, the best fitting is 0.06 ± 0.02 , which apparently confirms the presence of a positive correlation at the 3σ level. However, we note that the linear best-fit results are strongly dependent on the data points with count rate below $\sim 1 - 1.2$ count/s. These bins are scarcely populated. Indeed, if we take into account only the binned points that contain at least 8 data, the significance of the positive correlation disappears (see Table 1) and the HR values are not correlated with the count rate any more. This result is consistent with the findings from the previous section.

In summary, the results from the study of the $HR - ct$ plots confirm the findings from the study of the flux-flux plots. The spectral behavior of the source is identical on different time scales. We find no significant evidence for positive or negative correlations between hardness ratio and total count rate. As before, this result suggests that the flux variations occur while the continuum spectral shape remains constant.

We do note though that there is a hint of a weak, positive trend between the hardness ratios and flux, in the sense that the spectrum hardens as the source brightens. This trend is more obvious at low flux levels. We need to accumulate more data points at high and (mainly) low count rates, in order to be able to confirm (or refute) this hypothesis on statistical grounds.

4.3. Fractional Variability vs. Energy

Another simple way to quantify the variability properties of PKS 0558–504 without considering the time ordering of the values in the light curves, is based on the fractional variability parameter F_{var} (e.g. Rodriguez-Pascual et al. 1997; Vaughan et al. 2003). This is a commonly used measure of the intrinsic variability amplitude relative to the mean count rate, corrected for the effect of random errors, i.e.,

$$F_{\text{var}} = \frac{(\sigma^2 - \Delta^2)^{1/2}}{\langle r \rangle} \quad (1)$$

where σ^2 is the variance, $\langle r \rangle$ the unweighted mean count rate, and Δ^2 the mean square value of the uncertainties associated with each individual count rate. The error on F_{var} has been estimated following Vaughan et al. (2003):

$$\sigma_{F_{\text{var}}} = \sqrt{\left(\sqrt{\frac{1}{2N}} \cdot \frac{\Delta^2}{\langle r \rangle^2 F_{\text{var}}} \right)^2 + \left(\sqrt{\frac{\Delta^2}{N}} \cdot \frac{1}{\langle r \rangle} \right)^2} \quad (2)$$

where N is the number of data points.

We computed F_{var} on selected energy bands. These bands were chosen in such a way to have mean count rates similar and sufficiently high. A separate analysis for S1 and S2 suggests a similar behavior for the two data sets. This conclusion is confirmed in a more quantitative way by computing the difference $\sum_i |F_{\text{varS1}}(E_i) - F_{\text{varS2}}(E_i)|$ over all energies, which yielded 0.43 ± 0.17 , which is a 2.5σ effect.

Having established that $F_{\text{var}}(\text{S1}) \sim F_{\text{var}}(\text{S2})$, we can estimate the F_{var} at each energy for the combined data set, using time bins of two days. The results, plotted in Fig. 5, suggest that in PKS 0558–504, the fractional variability amplitude is nearly constant between 2 and 15 keV. These findings are consistent with the results from the previous sections in that they indicate that there exist no flux-related, large amplitude spectral variations.

5. TIME-RESOLVED SPECTRAL ANALYSIS

Since the data consist of short snapshots spanning a long temporal baseline, they are well suited for monitoring the spectral variability of PKS 0558–504 but, in principle, not for a time-averaged spectral analysis. Nevertheless, since the spectral variability is not very pronounced (see §4), we have carried out a time-resolved spectroscopy by averaging spectra over two-month intervals. This choice is a trade-off between the necessity of accumulate sufficient counts for a reliable spectral analysis and the need to use limited temporal intervals to minimize the effects of the slow drift in the PCA gain.

We fitted all six two-month spectra with a simple power-law (PL) model absorbed by Galactic N_{H} ($4.8 \times 10^{20} \text{ cm}^{-2}$). The model fits all the data reasonably well. The best-fit results are listed in Table 2 and, as an example, Fig. 6 shows the best-fit PL model (together with the best-fit residuals) to the first 2-month long spectrum of the source.

Assuming $H_0 = 71 \text{ km s}^{-1} \text{ Mpc}^{-1}$, $\Omega_{\Lambda} = 0.73$ and $\Omega_{\text{M}} = 0.27$ (Bennet et al. 2003), the intrinsic luminosity is $L_{2-10 \text{ keV}} \sim 9 \times 10^{44} \text{ erg s}^{-1}$ (the corresponding flux is reported in Table 2), which corresponds to a sizable fraction ($> 15\%$) of the Eddington luminosity and causes the bolometric luminosity to exceed significantly L_{Edd} if we assume that $L_{2-10 \text{ keV}} \sim 0.05 - 0.10 L_{\text{bol}}$.

The best-fit spectral slope values are rather steep, as expected for a NLS1 object. They are all consistent within the errors, suggesting that there are no spectral variations, in agreement with the results in §4. Furthermore, we find no evidence for a second spectral component nor for the presence of an Fe $K\alpha$ line in any of the spectra. Adding a Gaussian line at 6.4 keV to the PL continuum model does not improve the fit significantly in any of the six spectra.

In order to investigate the issue of spectral variability in PKS 0558–504 in greater detail, we also extracted energy spectra from each individual PCU2 pointing. All spectra are reasonably well fitted by a simple power law absorbed by Galactic N_{H} . In Figure 7 we plot the best-fit Γ versus time for both the individual pointings (gray crosses) and the 2-month averaged spectra (black filled circles). Clearly, this plot suggests that the continuum spectral shape does not change with time. We estimate a $\chi^2 = 164.7$ for 207 dof and a $\chi^2 = 2.7$ for 5 dof in the case of the individual and the 2-month averaged Γ light curves, respectively. The weighted averages for the photon index are $\langle\Gamma\rangle = 2.20 \pm 0.03$ for the 2-month intervals and $\langle\Gamma\rangle = 2.23 \pm 0.02$ for the individual spectra.

Despite the absence of substantial spectral variability, a time-averaged analysis of the whole monitoring campaign is not feasible, because the continuous drift in the detector gain hampers the creation of an appropriate response matrix. Nevertheless, we have tried to exploit spectrally all the available data by fitting simultaneously the six 2-month averaged spectra. The resulting photon index is $\Gamma = 2.20 \pm 0.3$, fully consistent with the weighted mean. However, no tighter constraints on the presence of the Fe K line are obtained with this analysis.

In conclusion, we find that the spectrum of PKS 0558–504 is well fitted by a simple PL model with steep photon index, and shows no spectral slope variations.

6. DISCUSSION

We have used data from a year-long *RXTE* monitoring campaign to study the spectral variability of PKS 0558–504 following model-independent and spectral model fitting methods. The main results can be summarized as follows:

- The light curves (Fig. 2) show large amplitude variations on time scales ranging between half a day to several days/weeks, independently of the sampling pattern and energy range. Indeed, the fractional variability F_{var} is of the order of 25-30% in all energy bands (Fig. 5).
- The large amplitude flux variations are not accompanied with substantial spectral variations. We do observe some low amplitude spectral variations, but they are not flux correlated (as both the flux vs flux and $HR - ct$ plots show). There is a hint of a positive trend in the $HR - ct$ plot, mainly at low fluxes (Fig. 4) but more data are needed to confirm this result.
- The spectra, both from individual orbits and from the 2-month averaged data, are well fitted by a power-law model, with $\langle\Gamma\rangle \simeq 2.2$. This average value is the same for both S1 (long time scales) and S2 (short time scales) data sets.
- We find no indication of an iron line, in any of the 2-month averaged or individual spectra. The weakness of the reflection features in the 2–15 keV range is confirmed by the flux-flux plot (Fig. 3). The almost zero intercept in the flux-flux plot suggests a negligible contribution from a constant reflection component which is usually observed in other Seyfert galaxies.

The time-averaged spectral results of PKS 0558–504 ($\Gamma = 2.2$, $EW < 50$ eV), obtained in the 2.5–15 keV energy range during the *RXTE* monitoring campaign, are in broad agreement with the findings obtained by previous X-ray missions. A compilation of the measured photon indices of PKS 0558–504 over one decade is reported in Gliozzi et al. (2000): with the exception of *ROSAT* ($\Gamma \simeq 3.1$; Brinkmann et al. 1997) that only probes the soft range 0.1–2.4 keV, all the values obtained by *GINGA* ($\Gamma \simeq 2.24$; Remillard et al. 1991), *EXOSAT* ($\Gamma \simeq 2.21$; Lawson et al. 1992), and *ASCA* ($\Gamma \simeq 2.25$; Leighly et al. 1999) are consistent with the *RXTE* findings, suggesting that the spectrum of PKS 0558–504 has remained roughly constant for more than 15 years. The average spectral slope measured with *RXTE* is also in good agreement with the best-quality spectral data to date obtained with *XMM-Newton* in the 2–10 keV range (2.12 ± 0.15 ; O’Brien et al. 2001). In addition to PKS 0558–504, Leighly (1999) presents a comprehensive analysis of 22 NLS1 observed by *ASCA*, showing that the photon index of PKS 0558–504 is fully consistent with the average Γ of the NLS1 sample. On the other hand, the equivalent width of an Fe K line of PKS 0558–504 measured by *ASCA* ($EW = 106$ eV) has the lowest value among the NLS1 with detected lines (but see Ballantyne et al. 2002 for a different interpretation of the *ASCA* data). The weakness of the Fe K line is also consistent with the low upper limits obtained by *XMM-Newton*: < 10 eV for a narrow line ($\sigma = 10$ eV) and < 90 eV for a broad line ($\sigma = 300$ eV; O’Brien et al. 2001).

The *RXTE* spectral variability findings (large flux changes without substantial spectral variations) can be compared with the work of Brinkmann et al. (2004), who present the results from several *XMM-Newton* observations of PKS 0558–504 carried out over a period of almost two years. Despite the fact that the *XMM-Newton* observations are carried out in a different energy band (0.2–10 keV versus 2.5–15 keV in our case) and probe shorter time scales, we find a remarkable agreement with the *RXTE* results. In particular, Figure 4 of Brinkmann et al. (2004) shows that large amplitude count rate changes are not accompanied by a clear spectral trend, and that there is a substantial scatter in the hardness ratio values for a given count rate.

Since the primary goal of this work was to investigate the origin of the X-rays in PKS 0558–504 and in particular to assess the role played by the putative jet, it is instructive to compare our study with similar analyses carried out both on radio-quiet AGN (where the X-rays are thought to be produced by Comptonization in the corona that is closely connected with the accretion disk) and on radio-loud jet-dominated AGN (whose radiation over the entire energy range is ascribed to jet emission).

Previous studies of nearby radio-quiet AGN (including mostly broad-line Seyfert galaxies, but also NLS1), based

on yearly-long *RXTE* observations, have revealed a well defined spectral behavior, which is characterized by: 1) A nearly ubiquitous spectral softening when the source brightens (Papadakis et al. 2002; Markowitz & Edelson 2004). 2) A more pronounced variability in the soft (2–4 keV) band than in the hard (7–10 keV) energy range (Markowitz & Edelson 2001). 3) Time-resolved spectra with prominent reprocessing features: an Fe $K\alpha$ line is always statistically required by the fit and the reflection fraction R is typically of the order of 0.5 (Markowitz et al. 2003).

Also radio-loud jet-dominated AGN, such as the brightest blazars, have been targeted by several monitoring campaigns with *RXTE* in recent years. However, most of these studies are focused either on the interpretation of the broad-band spectral energy distribution or on the variability properties with structure functions and power density spectra (e.g., Kataoka et al. 2001). Recently, a model-independent study of the spectral variability properties of the nearby blazar Mrk 501 has been performed by Gliozzi et al. (2006a). Interestingly enough, Mrk 501 shows a markedly different spectral behavior compared to radio-quiet objects, with spectral variations characterized by a hardening when the source brightens, and with the fractional variability more pronounced at higher energies. The bluer when brighter behavior has been observed also in other blazars (see Rebillot et al. 2006 and references therein).

If we compare the spectral properties of PKS 0558–504 with those of radio-quiet AGN and blazar objects, we find that they are not consistent with the characteristic behavior of either AGN class. Despite the significant flux variations, PKS 0558–504 does not show any clear softening (or hardening) of the spectra when the count rate increases, nor does it present any marked energy dependence of F_{var} . This suggests that PKS 0558–504 is a remarkably peculiar object.

Another object that shows a similar spectral behavior is 3C 273. Long-term *RXTE* observations reveal a dual spectral behavior for 3C 273, with achromatic flux variations (which have been interpreted as associated with jet emission) during 1996–1997 and Seyfert-like spectral variations (softening of the spectrum when the source brightens) accompanied by Fe $K\alpha$ detections during 1999–2000 (Kataoka et al. 2002). This suggests, according to Kataoka et al. (2002), that 3C 273 is a hybrid object with contributions from the jet and the accretion-related component varying with time. However, it is not just 3C 273 that shows a similar achromatic variability behavior. For example, the radio-quiet quasar PG 0804+761 shows flux variations without any spectral variation associated and has an iron line at ~ 6.4 keV with $\text{EW} \sim 110$ eV in its spectrum (Papadakis et al. 2003).

The presence of a jet in PKS 0558–504, probably seen at a small viewing angle, is supported by the flat radio spectrum and the limited radio extension of the source at VLA resolution (Lucyna Kedziora-Chudczer private communication). In addition, the lack of reprocessing features in the *RXTE* PCA spectrum (the Fe K line is never detected at significant level and $\text{EW} \lesssim 50$ eV at a 90% confidence level) also favors the presence of a jet, which may actually be the dominant source of X-ray emission. This conclusion

can find further support from the similarity of PKS 0558–504 with 3C 373 during its supposedly jet-dominated period that is characterized by substantial flux changes without spectral variability. Note that, contrary to PKS 0558–504, 3C 373 sometimes shows a fairly strong Fe K line in its spectrum ($\text{EW} \simeq 100\text{--}200$ eV) and Seyfert-like spectral variations, suggesting that PKS 0558–504 might be more jet-dominated than 3C 273.

In the framework of jet-dominated models, flux variations without relevant spectral changes can be naturally explained by changes in the electron injection rate (Kirk, Rieger, & Mastichiadis 1998) or by changes in the orientation of the jet (e.g., Villata & Raiteri 1999).

Alternatively, in the framework of (thermal) coronal models, the spectral variability is essentially regulated by two parameters: the temperature kT and the optical depth τ . In principle, one might reproduce the peculiar spectral variability shown by PKS 0558–504 by assuming that the respective changes in kT and τ cancel out. However, considering the large amplitude flux variations observed in PKS 0558–504, we regard this hypothesis as unlikely, since it requires fine tuning.

Nonetheless, coronal models may still represent a viable solution for PKS 0558–504, if we allow for changes in the supply of seed photons and variable power in the Comptonized component (see Gierliński & Zdziarski 2005 and references therein). Indeed, spectral behaviors quite similar to the one shown by PKS 0558–504 (in particular, $F_{\text{var}}(E) = \text{constant}$) have been observed in Galactic black hole systems (GBHs) during their transition from the hard to the soft spectral state, and interpreted in the framework of coronal models (Gierliński & Zdziarski 2005). Interestingly, in this scenario, PKS 0558–504 would be associated with GBHs in their intermediate states, where sometimes transient relativistic jets are observed (Fender, Belloni, & Gallo 2004). In the coronal scenario, the complete lack of reprocessing features in the energy spectra of PKS 0558–504 might be explained by extreme relativistic blurring (Crummey et al. 2006) or by very strong Comptonization (Matt et al. 1997).

In summary, PKS 0558–504 shows unique X-ray properties, which are not similar to what most (but not all) of radio-quiet Seyferts and blazars show. It looks similar to 3C 273 (during the supposedly jet-dominated period), in the sense that this source also does not show spectral variations, but the average Γ in 3C 273 is much flatter than in PKS 0558–504. It also looks similar to the radio-quiet quasar PG 0804+761, and in this case, also the spectral slopes are similar. However, contrary to PKS 0558–504, PG 0804+761 shows a standard Fe $K\alpha$ line. If jet emission is dominant, then the jet varies in a non-standard way (as otherwise, PKS 0558–504 should show the bluer when brighter behavior). If the corona is dominant, then again, the source must be in this “rare” intermediate state, as it is different to most of the other Seyfert galaxies (both broad and narrow-lined). In either case, PKS 0558–504 is a rare source, a very interesting one. With the new data from the current observations, we will: a) check that the first year results are indeed representative of the source’s behavior, b) we will study better the possibility of weak flux related spectral variations, and c) we will study the flux variations in terms of power spectrum analysis. This

will help us decide which mechanism is dominant in the X-rays.

MG acknowledges support by the RXTE Guest Investigator Program under NASA grant 200857. IEP and WP

gratefully acknowledge travel support through the bilateral Greek-German IKYDA project based personnel exchange program. We thank the referee for his comments and suggestions that improved the clarity of the paper.

REFERENCES

- Arnaud, K. 1996, in ASP Conf. Ser. 101, *Astronomical Data Analysis Software and Systems V*, ed. G. Jacoby & J. Barnes (San Francisco: ASP), 17
- Ballantyne, D.R., Iwasawa, K., & Fabian, A.C. 2001, *MNRAS*, 323, 506
- Bennet, C.L. et al. 2003, *ApJS*, 148, 1
- Bevington, P.R. 1969. *Data Reduction and Error Analysis for the Physical Sciences*. McGraw-Hill, New York
- Boller Th., Brandt W.N., Fabian A.C., Fink H.H. 1997, *MNRAS* 289, 393
- Boroson, T.A. & Green, R.F. 1992, *ApJS*, 80, 109
- Brandt W.N., Boller Th., Fabian A.C., Ruzkowski M. 1999, *MNRAS* 303, L53
- Brinkmann, W., Yuan, W., & Siebert, J. 1997, *A&A*, 319, 413
- Brinkmann, W., Arévalo, P., Gliozzi, M., Ferrero, E. 2004, *A&A*, 415, 959
- Crummy, J., Fabian, A.C., Gallo, L., Ross, R.R. 2006, *MNRAS*, 365, 1067
- Churazov, E., Gilfanov, M., & Revnivtsev, M. 2001, *MNRAS*, 321, 759
- Fender R.P., Belloni, T.M., & Gallo, E. 2004, *MNRAS*, 355, 1105
- Fossati, G., Celotti, A., Chiaberge, M., et al. 2000, *ApJ*, 541, 153
- Forster K. & Halpern J.P. 1996, *ApJ* 468, 565
- Gallo, L.C., Tanaka, Y., Boller Th. 2004, *MNRAS*, 353, 1064
- Gierliński, M. & Zdziarski, A.A. 2005, *MNRAS*, 363, 1349
- Gliozzi M., Boller Th., Brinkmann W., Brandt W.N. 2000 *A&A* 356, L17
- Gliozzi M., Brinkmann, W., O'Brien, P.T., et al. 2001, *A&A* 365, L128
- Gliozzi M., Sambruna, R.M., Jung, I., et al. 2006a, *ApJ*, 646, 61
- Gliozzi M., Papadakis, I.E., R  th, C. 2006b, *A&A*, 449, 969
- Goodrich, R.W. 1989, *ApJ* 342, 224
- Grupe D., Beuermann K., Mannheim K., Thomas H.-C. 1999, *A&A* 350, 805
- Grupe D., Leighly K.M., Thomas H.-C., Laurent-Muehleisen S.A. 2000, *A&A* 356, 11
- Grupe D., Thomas, H.-C., & Beuermann, K. 2001, *A&A*, 367, 470
- Grupe D. 2004, *AJ*, 127, 1799
- Grupe, D. & Mathur, S. 2004, *ApJ*, 606, 41
- Jahoda, K., Swank, J., Giles, A.B., et al. 1996, *Proc.SPIE*, 2808, 59
- Kataoka, J., Takahashi, T., Wagner, S.J., et al. 2001, *ApJ*, 560, 659
- Kataoka, J., Tanihata, C., Kawai, N., et al. 2002, *MNRAS*, 336, 932
- Kaspi, S., Smith, P.S., Netzer, H., et al. 2000, *ApJ*, 533, 631
- Kirk, J.G., Rieger, F.M., & Mastichiadis, A. 1998, *A&A*, 333, 452
- Komossa, S., Voges, W., Xu, D., et al. 2006, *AJ*, 132, 531
- Aharonian, F., 2002, *MNRAS*, 336, 721
- Lawson, A.J. & Turner, M.J.L. 1997, *MNRAS*, 288, 920
- Leighly, K.M. 1999, *ApJS*, 125, 297
- Leighly, K.M. 1999, *ApJS*, 125, 317
- Markoff, S., Nowak, M., Corbel, S., Fender, R., & Falcke, H. 2003, *NewAR*, 47, 491
- Markowitz, A. & Edelson, R. 2001, *ApJ*, 547, 684
- Markowitz, A., Edelson, R., & Vaughan, S. 2003, *ApJ*, 598, 935
- Markowitz, A. & Edelson, R. 2004, *ApJ*, 617, 939
- Mathur S. 2000, *MNRAS*, 314, L17
- Matt, G., Fabian, A.C., & Reynolds, C.S. 1997, *MNRAS*, 289, 175
- Mirabel, I.F. & Rodr  guez, L.F. 1994, *Nature*, 371, 46
- Moran E.C., Halpern J.P., Helfand D.J. 1996, *ApJS* 106, 341
- O'Brien, P.T., et al. 2001, *A&A*, 365, L122
- Osterbrock, D.E. & Pogge, R.W. 1985, *ApJ*, 297, 166
- Papadakis, I.E., Petrucci, P.O., Maraschi, L., et al. 2002, *ApJ*, 573, 92
- Papadakis, I.E., Reig, P., & Nandra, K. 2003, *MNRAS*, 344, 993
- Press, W.H., Teukolsky, S.A., Vetterling, W.T., & Flannery, B.P. 1997, *Numerical Recipes* (Cambridge: Cambridge Univ. Press)
- Puchnarewicz, E.M., Mason, K.O., Cordova, F.A. et al. 1992, *MNRAS*, 256, 589
- Rebillot, P.F., et al. 2006, *ApJ*, 641, 740
- Remillard R.A., Bradt H.V., Buckley D.A.H., Roberts W., Schwartz D.A., et al., 1986, *ApJ* 301, 742
- Remillard R.A., Grossan B., Bradt H.V., Ohashi T., Hayashida K., et al., 1991, *Nat* 350, 589
- Rodr  guez-Pascual, P.M., Alloin, D., Clavel, J., et al. 1997, *ApJS*, 110, 9
- Rotschild, R.E., Blanco, P.R., Gruber, D.E., et al. 1998, *ApJ*, 496, 538
- Siebert J., Leighly K.M., Laurent-Muehleisen S.A. Brinkmann W., Boller Th., Matsuoka M. 1999, *A&A* 348, 678
- Sulentic, J.W., Zwitter, T., Marziani, P., Dultzin-Hacyan, D. 2000, *ApJ*, 536, 5
- Taylor, R.D., Uttely, P., & McHardy, I.M. 2003, *MNRAS*, 342, 31
- Ulvestad J.S., Antonucci R.R.J. Goodrich R.W. 1995 *AJ* 109, 81
- Vaughan, S., Edelson, R., Warwick, R.S., & Uttley, P. 2003, *MNRAS*, 345, 1271
- Villata, M. & Raiteri C.M. 1999, *A&A*, 347, 30
- Wang, T.G., Matsuoka, M., Kubo, H., Mihara, T., Negoro, H. 2001, *ApJ*, 554, 233
- Zdziarski, A.A., Gierliński, M., Miko?ajewska, J., et al. 2004, *MNRAS*, 351, 791

TABLE 1
MODEL-INDEPENDENT SPECTRAL VARIABILITY

Flux – Flux				
Data	Slope	Intercept	χ^2/dof	P_{χ^2}
unbinned	0.74±0.03	0.02±0.02	218.7/139	1.9×10^{-5}
binned	0.76±0.03	0.00±0.03	8.7/7	2.8×10^{-1}
HR – rate				
unbinned	0.05±0.02	0.68±0.03	172.6/138	2.4×10^{-2}
binned	0.06±0.02	0.65±0.03	30.2/14	7.1×10^{-3}
binned♣	0.02±0.03	0.73±0.06	5.8/5	3.2×10^{-1}

♣ Only bins well populated (> 8 data points) are considered

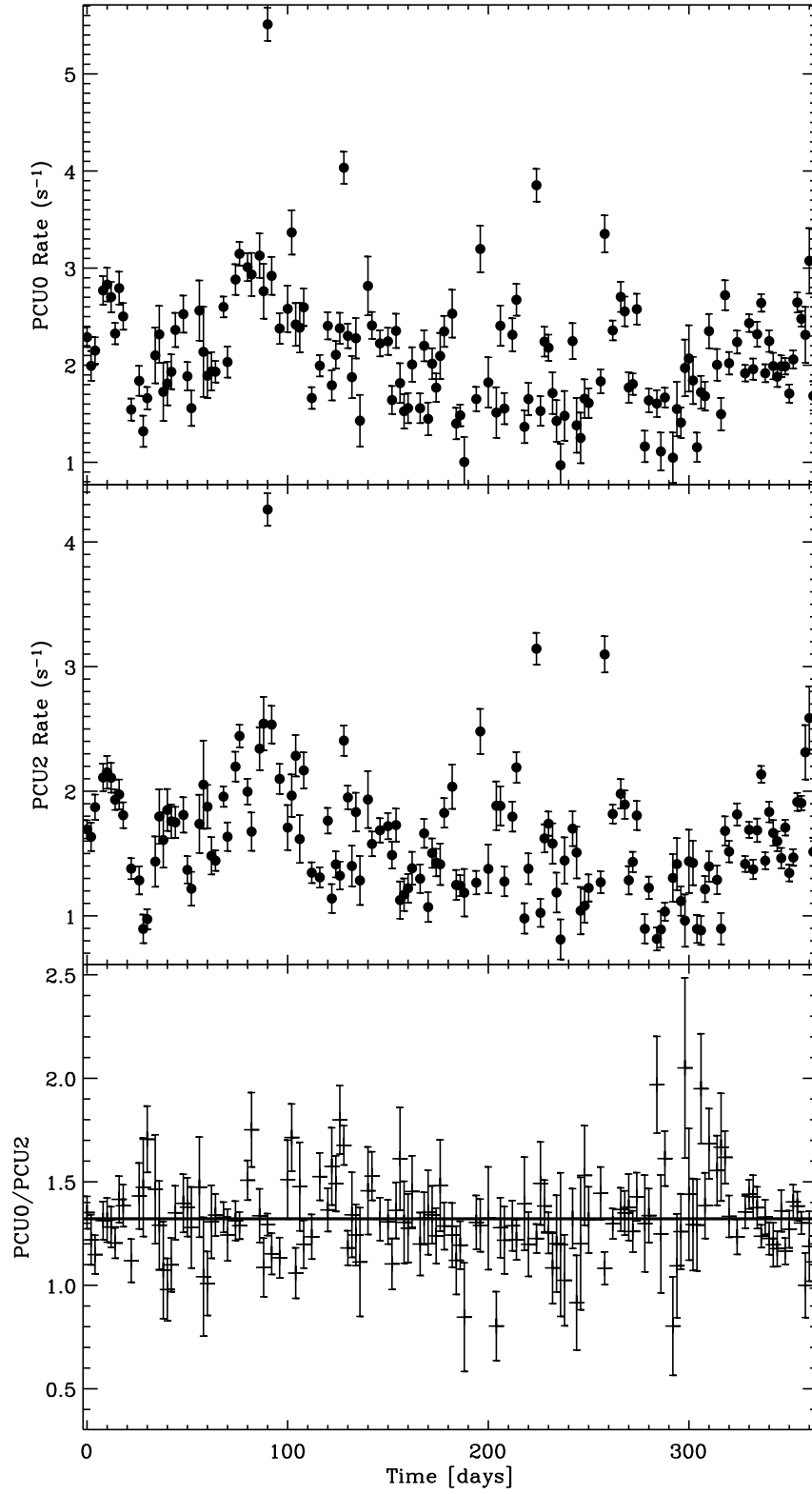


FIG. 1.— Top panel: PCU0 light curve of PKS 0558–504 in the 2–15 keV range. Middle panel: PCU2 light curve of PKS 0558–504 in the 2–15 keV range. Bottom panel: PCU0/PCU2 light curve; the solid line represents the average value of the ratio PCU0/PCU2. Time bins are two days. The reference time corresponding to Time = 0 is 2005 March 4 UT 09:05:15.

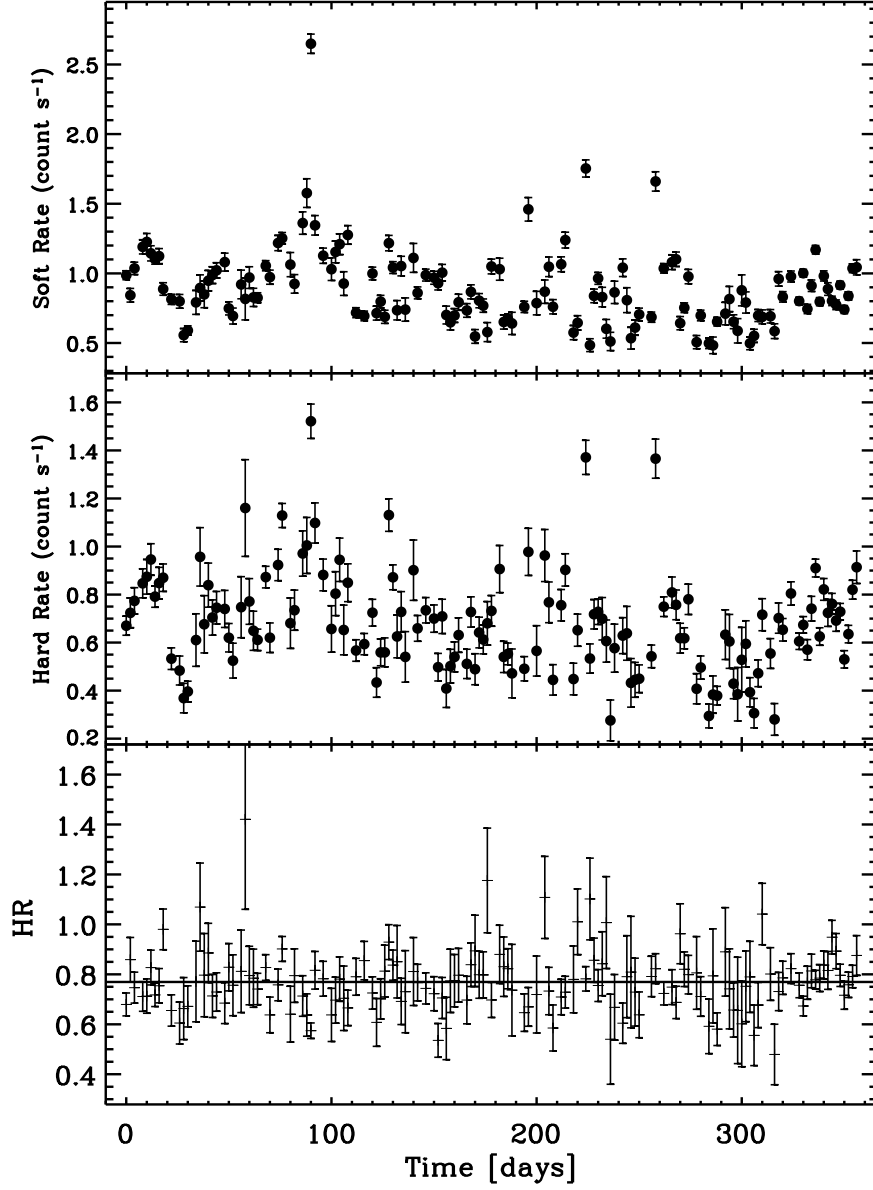


FIG. 2.— Top panel: Soft (2.5–5 keV) light curve of PKS 0558–504 using PCU2 data only. Middle panel: Hard (5–15 keV) light curve. Bottom panel: Hardness Hard/Soft ratio light curve; the solid line represents the average value of the hardness ratio. Time bins are two days.

TABLE 2
SPECTRAL ANALYSIS RESULTS

Interval (yy/mm/dd)	χ^2/dof	$F_{2-10 \text{ keV}}$ ($10^{-11} \text{ erg cm}^{-2} \text{ s}^{-1}$)	Γ	$\text{EW}_{\text{FeK}\alpha}$ (eV)
05/03/04-05/05/03	15.6/25	1.88	$2.21^{+0.09}_{-0.14}$	< 155
05/05/05-05/07/04	18.6/25	2.20	$2.25^{+0.07}_{-0.07}$	< 68
05/07/06-05/09/04	32.1/25	1.77	$2.18^{+0.08}_{-0.07}$	< 35
05/09/06-05/11/05	22.9/25	1.77	$2.17^{+0.11}_{-0.11}$	< 52
05/11/07-06/01/06	31.8/25	1.54	$2.22^{+0.08}_{-0.10}$	< 48
06/01/08-06/03/02	31.7/25	1.88	$2.18^{+0.05}_{-0.05}$	< 50

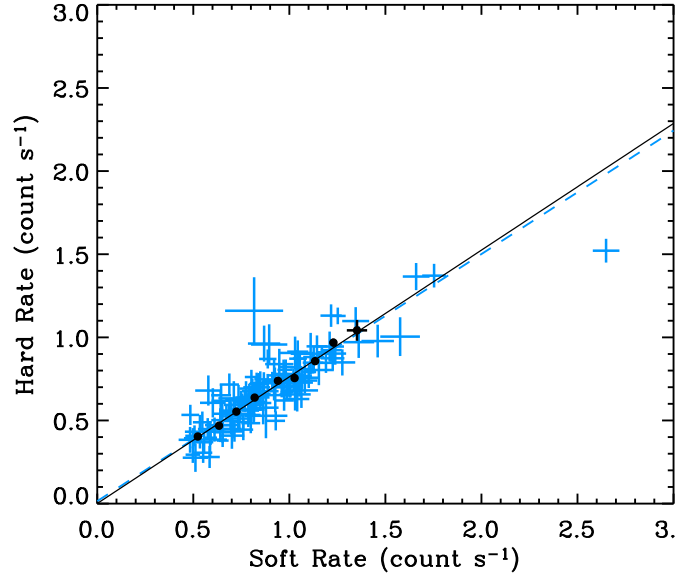


FIG. 3.— Flux-flux plot of PKS 0558-504. The soft count rate refers to the 2.5–5 keV band, the hard to the 5–15 keV band. The gray (blue in color) symbols correspond unbinned data points, whereas the black filled circles refer to the weighted mean of the original points with fixed bins of 0.1 c/s. The outlier corresponds to the point with the highest count rate occurring ~ 90 days after the beginning of the monitoring campaign. The gray dashed line represents the best-fit linear model for the unbinned points, whereas the black continuous line refers to the binned data points.

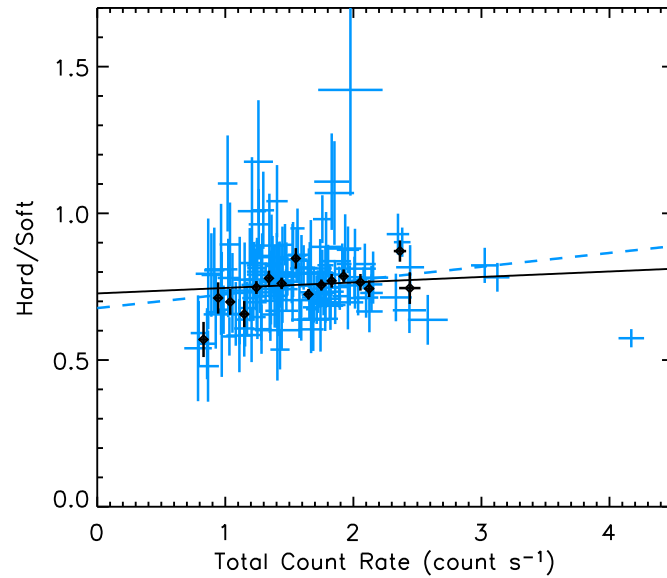


FIG. 4.— Hardness ratio (5–15 keV/2.5–5 keV) plotted versus the count rate. The gray (blue in color) crosses refer to unbinned data, whereas the black filled circles correspond to weighted means of the original points with fixed bins of 0.1 c/s. The gray dashed line represents the best-fit linear model for the unbinned points, whereas the black continuous line refers to the (well-populated) binned data points; see text for more details.

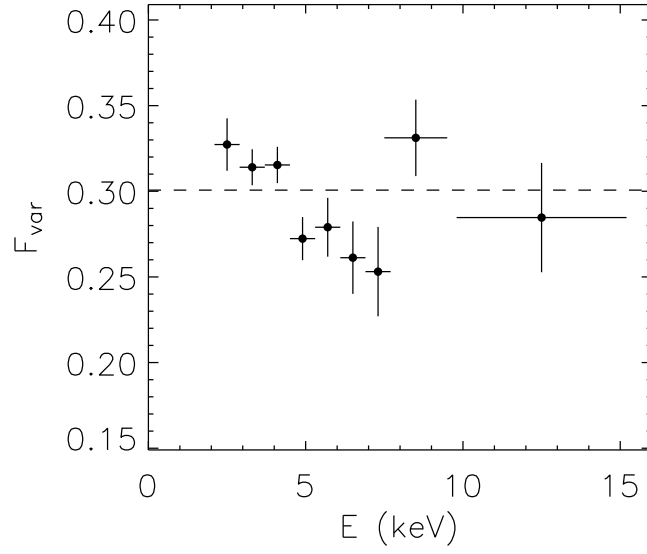


FIG. 5.— Fractional variability amplitude as a function of energy for PKS 0558–504. The error-bars along the x axis simply represent the energy band width. The error bars along the y axis are computed following Vaughan et al. 2003. The dashed line represents the weighted mean of F_{var} .

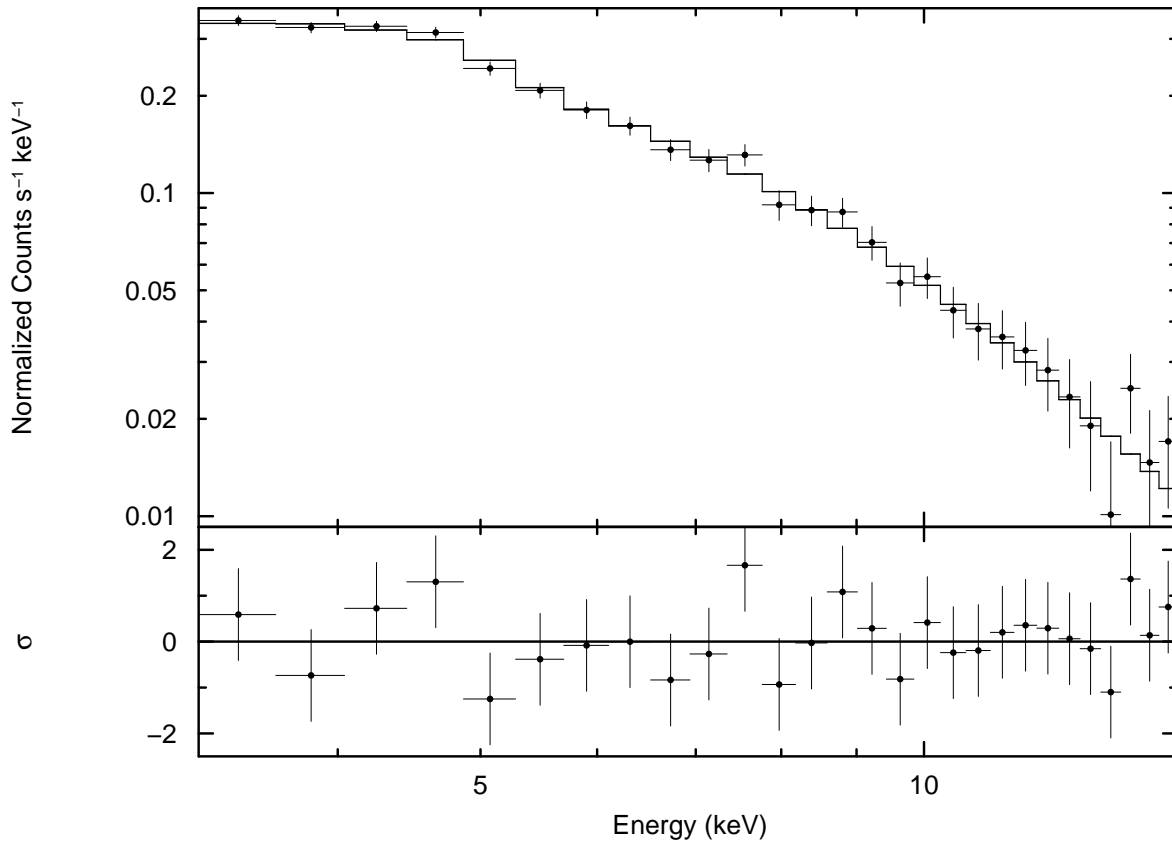


FIG. 6.— PCA spectrum of PKS 0558–504 during the first 2-month interval obtained using PCU2 data only

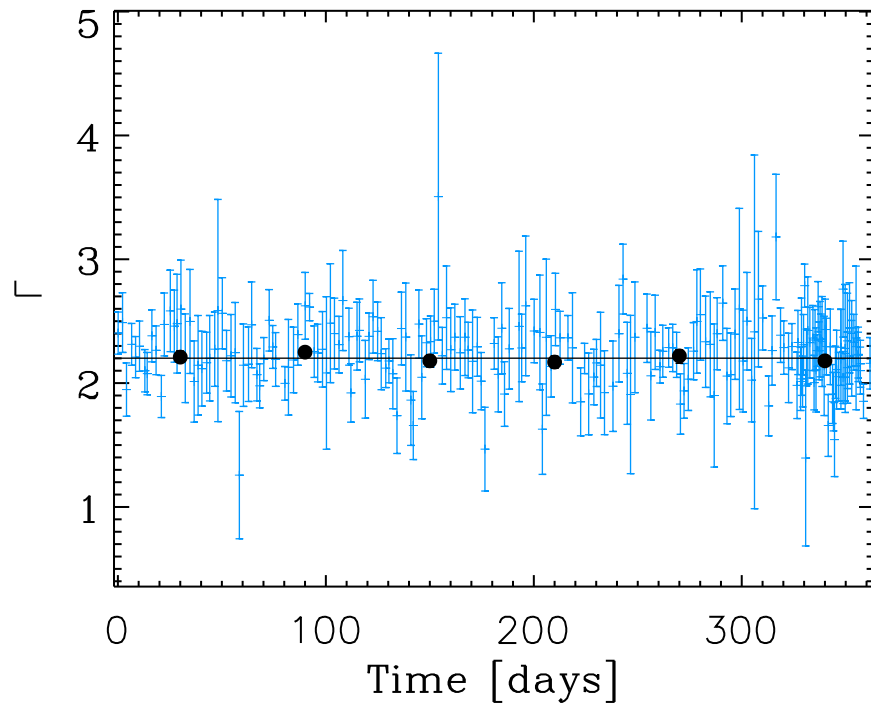


FIG. 7.— Gray (blue in color) symbols represent the values of Γ obtained in individual pointings plotted against time. Black filled circles refers to 2-month averaged spectra. All error-bars are 1σ . The solid line represent the mean value obtained averaging the 2-month spectra.